



# Cosmic Clues from Amaterasu: Blazar-driven Ultrahigh-energy Cosmic Rays?

Saikat Das<sup>1</sup> , Srijita Hazra<sup>2</sup> , and Nayantara Gupta<sup>2</sup> <sup>1</sup> Department of Physics, University of Florida, Gainesville, FL 32611, USA; [saikatdas@ufl.edu](mailto:saikatdas@ufl.edu)<sup>2</sup> Astronomy & Astrophysics Group, Raman Research Institute, Sadashivanagar, Bangalore 560080, Karnataka, India

Received 2025 April 19; revised 2025 June 7; accepted 2025 June 16; published 2025 July 15

## Abstract

The detection of the Amaterasu event of energy 244 EeV by the Telescope Array, one of the most energetic ultrahigh-energy cosmic rays (UHECRs;  $E \gtrsim 0.1$  EeV) observed to date, invites scrutiny of its potential source. We investigate whether the nearby blazar PKS 1717+177 at redshift  $z = 0.137$ , located within  $2.5^\circ$  of the reconstructed arrival direction, could explain the event under a proton-primary hypothesis. Using a one-zone jet model, we fit the multiwavelength spectral energy distribution of the source, incorporating both leptonic and hadronic cascade emissions from photohadronic interactions inside the jet. Our model supports a cosmic-ray origin of the very-high-energy ( $\varepsilon_\gamma \gtrsim 100$  GeV)  $\gamma$ -ray flux and predicts a subdominant neutrino flux, 1 one order of magnitude lower than from TXS 0506+056. Under Lorentz invariance violation, UHECRs escaping the blazar jet above a specific energy can propagate unattenuated over hundreds of Mpc due to an increase in energy loss length for certain parameter choices. In such a scenario, the Amaterasu event can have a plausible origin from this blazar. Our analysis indicates negligible deflection in the Galactic magnetic field, implying a strong extragalactic magnetic field is required. Our findings provide a compelling multimessenger framework linking UHECRs,  $\gamma$ -rays, and neutrinos and motivate targeted searches by current and future high-energy neutrino telescopes during increased  $\gamma$ -ray or X-ray activity of this blazar.

*Unified Astronomy Thesaurus concepts:* High energy astrophysics (739); Active galactic nuclei (16); Gamma-ray astronomy (628); Ultra-high-energy cosmic radiation (1733); Neutrino astronomy (1100); Blazars (164)

## 1. Introduction

The origin of ultrahigh-energy cosmic rays (UHECRs;  $E \gtrsim 10^{17}$  eV) is an unsolved enigma in astrophysics (see K. Kotera & A. V. Olinto 2011; L. A. Anchordoqui 2019, for review). Unlike  $\gamma$ -rays and neutrinos, their sources are obscured by deflections in cosmic magnetic fields (see, e.g., G. Sigl et al. 2004; N. Globus et al. 2008). Observed features in their energy spectrum suggest a distinct extragalactic source population. However, the exact transition energy between Galactic and extragalactic cosmic rays is still unknown (e.g., R. Aloisio et al. 2012). The leading experiments observing these particles are the Pierre Auger Observatory in Argentina (Pierre Auger Collaboration 2015a) and the Telescope Array (TA) in Utah, USA (Telescope Array Collaboration 2016).

The detection of the “Oh-My-God” particle with an energy of  $\approx 320$  EeV by the Fly’s Eye experiment is the most energetic event recorded using the fluorescence technique, capturing the air shower due to the interaction with Earth’s atmosphere (D. J. Bird et al. 1995). However, the advent of water Cherenkov surface detector arrays has boosted the duty cycle of UHECR detection. The “Amaterasu” event observed by TA on 2021 May 27, named after the Shinto Sun goddess for its brilliance, is one of the most energetic cosmic-ray events detected by the surface detector. The estimated reconstructed energy of  $244 \pm 29$  (stat) $_{-76}^{+51}$  (sys) EeV and direction (R.A., decl.) =  $(255.9 \pm 0.6, 16.1 \pm 0.5)$  places it among the most energetic particles ever observed (Telescope Array Collaboration 2023).

The detection of such an extreme-energy event raises important questions regarding the nature and location of its source. The Griesen–Zatsepin–Kuz’min (GZK) suppression (K. Greisen 1966; G. T. Zatsepin & V. A. Kuz’min 1966) limits the observed UHECR energy due to photopion production off the cosmic microwave background (CMB). The energy-loss mean free path of protons at this energy is  $\mathcal{O} \sim 10$  Mpc (see, e.g., C. D. Dermer et al. 2009). UHECR composition studies by TA suggest light nuclei at  $\gtrsim 10^{19}$  eV, with significant uncertainties (R. U. Abbasi et al. 2010). A combined fit of the spectrum and composition by Auger suggests progressively heavier nuclei at  $\gtrsim 10^{18.2}$  eV (Pierre Auger Collaboration 2017). The maximum proton fraction in the highest-energy bin of the UHECR spectrum can go up to  $\sim 10\%$ – $15\%$  (M. S. Muzio et al. 2019; S. Das et al. 2021b; D. Ehlert et al. 2024). If the Amaterasu event originated within the local GZK horizon for protons, a source correlation is expected owing to the high magnetic rigidity. However, Amaterasu’s direction points to the Local Void, a region of the sky with a relatively small number of galaxies (R. B. Tully et al. 2008).

Ultraheavy UHECRs (B. T. Zhang et al. 2024), binary neutron star mergers (G. R. Farrar 2025), superheavy dark matter decay (K. Murase et al. 2025; P. Sarmah et al. 2025), the scattering of ultrahigh-energy (UHE) neutrinos by the cosmic neutrino background through Z-boson resonance (D. Fargion et al. 2024), starburst galaxy (N. Bourrache & F. Capel 2024), and a transient event in an unresolved Galaxy (M. Unger & G. R. Farrar 2024a) have been proposed for the astrophysical explanation of the Amaterasu event. UHECRs serve as a sensitive probe for testing Lorentz invariance violation (LIV; Pierre Auger Collaboration 2022), and such a possibility is also explored for this event (R. G. Lang 2024).



Original content from this work may be used under the terms of the [Creative Commons Attribution 4.0 licence](https://creativecommons.org/licenses/by/4.0/). Any further distribution of this work must maintain attribution to the author(s) and the title of the work, journal citation and DOI.

The reconstructed arrival direction of the Amaterasu event lies within  $2.5^\circ$  of the blazar PKS 1717+177 at redshift  $z = 0.137$ , assuming a proton primary. It is a nearby active galactic nucleus (AGN) identified in the  $\gamma$ -ray source catalog (Fermi-LAT Collaboration 2020). This flaring  $\gamma$ -ray source has been proposed as a neutrino-emitting AGN in point source stacking analysis of IceCube data (S. Britzen et al. 2024). AGNs have long been considered as sources of high-energy cosmic rays and neutrinos (see, e.g., D. Eichler 1979; V. S. Berezhinskii & V. L. Ginzburg 1981; M. Sikora et al. 1987; F. W. Stecker et al. 1991; K. Mannheim et al. 1992; A. P. Szabo & R. J. Protheroe 1994; A. Atoyan & C. D. Dermer 2001; K. Murase et al. 2014; S. Das et al. 2021a, 2022b; K. Murase & F. W. Stecker 2023). The detection of a high-energy neutrino by the IceCube Observatory in spatial and temporal coincidence with the flaring  $\gamma$ -ray blazar TXS 0506+056 corroborates cosmic-ray acceleration in jetted AGNs and its imprints on the multiwavelength spectrum (e.g., IceCube Collaboration 2018, IceCube Collaboration et al. 2018; S. Ansoldi et al. 2018; A. Keivani et al. 2018).

In this work, we show that UHE protons of energy  $\gtrsim 0.1$  EeV can be injected from the jet of this blazar. They undergo deflection in cosmic magnetic fields without suffering interactions beyond 10 EeV for a suitable choice of the LIV coefficient (Pierre Auger Collaboration 2022). However, the LIV effects are insignificant below tens of EeV energies. Hence, a hadronic signature in the  $\gamma$ -ray flux should be observed due to interactions inside the jet if this source accelerates cosmic rays.

A fit to the blazar spectrum using a leptohadronic model is obtained, including radiation from the electromagnetic cascade of secondary electrons. Our analysis reveals that the fit to very-high-energy (VHE;  $E \gtrsim 0.1$  TeV)  $\gamma$ -ray flux is improved compared to a purely leptonic model. The latter suffers from the Klein–Nishina effect, resulting in inefficient inverse-Compton scattering at the VHE regime. The estimated neutrino event rate is beyond the sensitivity of current detectors. The required kinetic power in protons constrains the rigidity cutoff required in the UHECR spectrum. We also analyze the deflection in cosmic magnetic fields, thus constraining the rms field strength of the extragalactic medium.

We present our analysis and results obtained in Section 3 and examine the implications for UHECR sources in Section 4. We draw our conclusions in Section 5.

## 2. Model Considerations

The broadband spectral energy distribution (SED) of the source is obtained from the archival data retrieved from the SSDC SED builder (G. Stratta et al. 2011). The radio data were obtained from CRATES (S. E. Healey et al. 2007), FIRST (R. H. Becker et al. 1994), NIEPPOCAT (E. Nieppola et al. 2007), PKSCAT90 (A. Wright & R. Otrupcek 1992), and PLANCK (Planck Collaboration et al. 2014). The infrared (IR) data were collected from the Wide-field Infrared Survey Explorer catalog (E. L. Wright et al. 2010). The data for optical-UV wave bands were collected from the UV and Optical Telescope (UVOT) of the Swift Observatory (P. Giommi et al. 2012) and the Galaxy Evolution Explorer (L. Bianchi et al. 2011) catalog. The X-ray data were found from Swift-X-ray Telescope (S. Britzen et al. 2024) and MAXI (T. Kawamuro et al. 2018). The Fermi 4FGL-DR4 (J. Ballet et al. 2023), along with earlier data releases, provides the  $\gamma$ -ray spectrum of the source.

We model the emission region of PKS 1717+177 as a spherical blob of radius  $R'$  embedded in the jet, consisting of a relativistic plasma of electrons and protons moving through a uniform magnetic field  $B'$  in the comoving jet frame. The jet has a bulk Lorentz factor  $\Gamma$ , and the Doppler factor is  $\delta_D = [\Gamma(1 - \beta \cos \theta)]^{-1}$ , where  $\beta c$  is the plasma velocity and  $\theta$  the viewing angle. For  $\theta \lesssim 1/\Gamma$ , we approximate  $\delta_D \approx \Gamma$ . Electrons are injected with a power-law distribution,

$$Q_e'(\gamma_e') = A_e(\gamma_e'/\gamma_0)^{-\alpha} \quad \text{for } \gamma_{e,\min}' < \gamma_e' < \gamma_{e,\max}', \quad (1)$$

to reproduce the observed broadband SED. Here,  $A_e$  depends on the injected electron luminosity, and  $\gamma_0 m_e c^2 = 500$  MeV is a reference energy. A quasi-steady state is achieved when the injection is balanced by radiative cooling and/or escape, yielding  $N_e'(\gamma_e') = Q_e'(\gamma_e') t_e'$  with  $t_e' = \min(t_{\text{cool}}', t_{\text{esc}}')$ , and  $t_{\text{esc}}' \simeq t_{\text{dyn}}' = 2R'/c$ . The cooling timescale is

$$t_{\text{cool}}' = 3m_e c / 4\sigma_T \gamma_e' (u_B' + \kappa_{\text{KN}} u_{\text{ph}}'), \quad (2)$$

where  $u_B' = B'^2/8\pi$ , and  $u_{\text{ph}}'$  is the soft photon energy density.  $\kappa_{\text{KN}}$  accounts for Klein–Nishina suppression of inverse-Compton emission. We solve the transport equation using the open-source code GAMERA (J. Hahn 2016; J. Hahn et al. 2022) to find the steady-state solution to

$$\frac{\partial N_e'}{\partial t} = Q_e'(\gamma_e', t') - \frac{\partial}{\partial \gamma_e'} (b N_e') - \frac{N_e'}{t_{\text{esc}}}, \quad (3)$$

where  $b(\gamma_e', t')$  is the energy loss rate. The steady-state electron spectrum produces synchrotron (SYN) and synchrotron self-Compton (SSC) emission. We include external inverse-Compton (EC) scattering of a blackbody photon field with temperature  $T'$  and comoving energy density  $u_{\text{ext}}' = (4/3)\Gamma^2 u_{\text{ext}}$ , where  $u_{\text{ext}} = \eta_{\text{ext}} L_{\text{disk}} / 4\pi R_{\text{ext}}^2 c$  is the energy density in the AGN frame, and  $\eta_{\text{ext}}$  is the fraction of the disk luminosity (A. Barnacka et al. 2014). The emission region is located at a distance  $R_{\text{ext}}$  along the jet axis. The external photons enter the jet and are Doppler-boosted in the comoving frame. The EC model provides a good fit to the entire broadband spectrum, suggesting that the source could be a masquerading BL Lac, i.e., an intrinsically flat-spectrum radio quasar with a hidden broad-line region (BLR) and a standard accretion disk, as proposed for TXS 0506+056 (P. Padovani et al. 2019).

We follow the numerical method described in S. Das et al. (2022a) and R. Prince et al. (2024) to model hadronic emission. The proton injection at the source is given by a power-law spectrum with a rigidity-dependent cutoff,

$$\frac{dN}{dE} = \begin{cases} A_p E_p^{-\alpha} & (E_p < ZR_{\text{max}}) \\ A_p E_p^{-\alpha} \exp\left(1 - \frac{E_p}{ZR_{\text{max}}}\right) & (E_p \geq ZR_{\text{max}}) \end{cases}. \quad (4)$$

For protons interacting in the blazar jet,  $E_p \ll R_{\text{max}}$ . Their dominant energy losses are through photopion production ( $p\gamma \rightarrow p + \pi^0$  or  $n + \pi^+$ ) and the Bethe–Heitler (BH) process ( $p\gamma \rightarrow p + e^+e^-$ ), with target photons originating from leptonic emission and external photon field. Charged pions decay to produce neutrinos. The interaction timescale is given by an integral over the photon distribution, cross section, and inelasticity as functions of photon energy in the proton rest frame (F. W. Stecker 1968; M. J. Chodorowski et al. 1992;

**Table 1**  
Leptohadronic Model Parameters for the Fit to Multiwavelength SED

$\delta_D$	$B'$ (G)	$R'$ (cm)	$u'_{\text{ext}}$ (erg cm <sup>-3</sup> )	$T'$ (K)	$\alpha$	$E_0$ (MeV)	$\gamma'_{e,\text{min}}$	$\gamma'_{e,\text{max}}$	$L_e$ (erg s <sup>-1</sup> )	$\gamma'_{p,\text{min}}$	$\gamma'_{p,\text{max}}$	$L_p$ (erg s <sup>-1</sup> )
25	1.0	$5 \times 10^{16}$	0.1	$5 \times 10^5$	2.0	500	20	$5 \times 10^4$	$4.1 \times 10^{42}$	10	$4.27 \times 10^6$	$1.3 \times 10^{45}$

**Note.** Electron and proton luminosities are in the AGN rest frame.

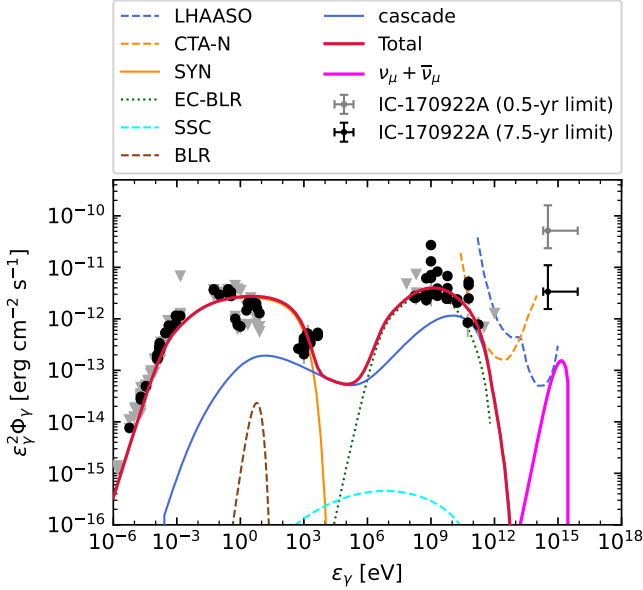


**Figure 1.** Multiwavelength SED of PKS 1717+177 showing the synchrotron (orange solid), external Compton (green dotted), the external photon field (brown dashed), the hadronic cascade (blue solid), and the  $\nu_\mu + \bar{\nu}_\mu$  spectrum (magenta) in the observer frame. Black data points show the spectral data from radio to VHE  $\gamma$ -rays, and upper limits are shown in gray. The black and gray error bars correspond to the neutrino flux from TXS 0506+056, which is shown for reference, assuming a 7.5 and 0.5 yr limit. The SSC spectrum shown in cyan color is negligible in the EC model. The orange dashed and blue dashed lines show the sensitivity of CTA-North and LHAASO detectors, respectively.

A. Mücke et al. 2000). Below a few PeV, the proton interaction timescale is longer than the dynamical timescale  $t'_{\text{dyn}}$ . To achieve a significant  $\pi^0$ -decay  $\gamma$ -ray flux, we model the escape rate such that it is smaller than the  $p\gamma$  interaction rate and hence can be neglected. The normalization  $A_p$  is set by the required kinetic power in protons.  $\gamma$ -ray and  $e^-$  spectrum from pion decay and  $e^\pm$  pairs from the BH process are calculated using the parameterization by S. R. Kelner & F. A. Aharonian (2008), weighting the input proton spectrum by the respective interaction rate. For example, to calculate the electron spectrum from BH interactions, protons are injected with a spectrum  $N'_p(\gamma'_p) \times R_{\text{BH}}/R_{\text{tot}}$ , where  $R_{\text{BH}}$  and  $R_{\text{tot}}$  are the BH and total (BH + photopion) interaction rates, respectively.

High-energy  $\gamma$ -rays undergo  $\gamma\gamma \rightarrow e^\pm$  absorption with soft photons and the external radiation field. The escaping TeV spectrum is thus suppressed as  $Q'_{\gamma,\text{esc}}(\epsilon'_\gamma) = Q'_{\gamma,\pi}(\epsilon'_\gamma)(1 - e^{-\tau_{\gamma\gamma}})/\tau_{\gamma\gamma}$ , where  $\tau_{\gamma\gamma}$  is the optical depth calculated following R. J. Gould & G. P. Schröder (1967), integrating over the target photon distribution and pair-production cross section. The high-energy  $\gamma\gamma$  pair production spectrum ( $Q'_{e,\gamma\gamma}$ ) is solved numerically using the expression in

M. Boettcher & R. Schlickeiser (1997). Together with the  $e^-$ -s from charged pion decay ( $Q'_{e,\pi}$ ) and BH process ( $Q'_{e,\text{BH}}$ ), they can initiate cascade radiation from the jet. We compute the steady-state spectrum  $N'_{e,s}$  of these electrons using the semianalytical approach of M. Boettcher et al. (2013), incorporating  $Q'_{e,\text{BH}}$  in the source term and using the same escape timescale as for primary electrons. In SYN-dominated cascades, the resulting photon spectrum is obtained by integrating over the electron distribution weighted by the SYN kernel  $Q'_s(\epsilon'_s) = A_0 \epsilon'^{-3/2} \int_1^\infty N'_{e,s}(\gamma'_e) \gamma'^{-2/3} e^{-\epsilon'_s/b\gamma'^2_e} d\gamma'_e$ , with  $A_0 = c\sigma_T B'^2/[6\pi m_e c^2 \Gamma(4/3)b^{4/3}]$  being a normalization constant, where  $b = B'/B_{\text{crit}}$  and  $B_{\text{crit}} = 4.4 \times 10^{13}$  G.

### 3. Results

#### 3.1. Multimessenger Emission

All model parameters were varied freely except the injection spectral index. A log-parabola injection spectrum was tested, but a simple power-law spectrum with  $\alpha = 2$  yields a satisfactory fit. Parameter degeneracy was assessed by scanning over a broad range of values. Given the multiple flux values at energies in the high-energy peak, we focused on the lower flux values to model the quiescent state. Earlier SED modeling of the source using older Fermi-Large Area Telescope (LAT) data (F. Tavecchio et al. 2010) suggests a hard LAT spectrum up to the highest energies, requiring a rather large Doppler factor,  $\delta > 50$ . We found that with improved spectral coverage across the radio to  $\gamma$ -ray band, the SSC model struggles to fit the entire data set consistently.

Although a leptonic inverse-Compton model remains feasible, we adopt a leptohadronic scenario motivated by the observed sub-TeV  $\gamma$ -ray emission. Moreover, including a hadronic component enables simultaneous reproduction of the highest-energy  $\gamma$ -ray and soft X-ray data through secondary electromagnetic cascades, which is difficult to achieve with leptonic emission alone. Here, we obtain  $\delta_D = 25$ , consistent with the SED fit up to the VHE regime.

We present the obtained best-fit parameter values in Table 1, considering a steady-state spectrum. The SED fit is shown in Figure 1, and the various components from leptonic and hadronic emission are labeled. The radius of the emission region  $R'$ , maximum electron Lorentz factor  $\gamma'_{e,\text{max}}$ , and the magnetic field  $B'$  are determined by fitting the optical and radio data with SYN emission (orange solid line). The latter peaks in the optical band, and a power-law injection spectrum of electrons provides a good fit to the data. The SYN radiation of muons and pions produced in hadronic interactions is not significant for  $B' = 1$  G. The high-energy peak constrains the temperature and energy density of the external photon field (brown dashed line), likely originating in the BLR region. They act as the most important target photon field for EC emission (green dotted line) as well as the  $p\gamma$  interaction of



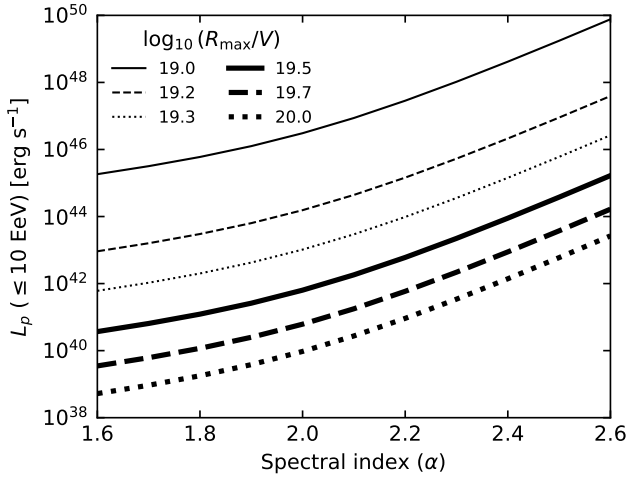


**Figure 2.** Proton luminosity in the 0.1 TeV to 10 EeV energy range constrained by the detection of 1 UHE proton event in the Telescope Array energy bin 148–340 EeV. The different curves correspond to various values of rigidity cutoff  $R_{\max}$  in the injection spectrum.

cosmic rays. This photon field also absorbs high-energy pion-decay  $\gamma$ -rays through  $\gamma\gamma$  pair production.

For a typical disk luminosity of  $10^{46} \text{ erg s}^{-1}$  and considering the scattered disk emission to be a fraction  $\eta_{\text{disk}} \sim 0.01$  of the disk photon energy density,  $R_{\text{ext}}$  comes out to be  $\sim 0.5 \text{ pc}$ . The secondary electromagnetic radiation (blue solid line) shows two peaks, viz., a lower energy peak from SYN radiation of secondary electrons, dominated by BH pairs, and a high-energy spectrum from pion-decay  $\gamma$ -rays. The VHE  $\gamma$ -ray data constrain the contribution from the pion-decay cascade and hence the proton spectrum normalization, limiting the peak flux of neutrinos. In the absence of hard X-ray data in the 10–100 keV range, the BH component of the hadronic cascade does not provide additional constraints (see, e.g., S. Das et al. 2022a; X. Jiang et al. 2025).

High-energy  $\gamma$ -ray absorption by the extragalactic background light (EBL), composed of optical, infrared, and ultraviolet photons, is included using the R. C. Gilmore et al. (2012) model. Observations by the Large High Altitude Air Shower Observatory (LHAASO; S. Vernetto 2016) and the Cherenkov Telescope Array (CTA; O. Gueta 2021) will further constrain the TeV  $\gamma$ -ray flux and hence the hadronic emission component. The orange dashed line in Figure 1 shows the differential point source sensitivity of the CTA northern array, assuming 50 hr observation time and pointing to  $20^\circ$  zenith angle. The blue dashed line shows the LHAASO 1 yr sensitivity to a Crab-like  $\gamma$ -ray point source.

A cutoff in the proton spectrum beyond a maximum energy  $E'_{p,\max}$  is required to explain the VHE spectrum. This also limits the peak energy of the neutrino spectrum. We assume protons above this energy escape the source, with an energy-independent escape timescale  $\sim R/c$  sufficient to suppress  $p\gamma$  interactions inside the jet. If the diffusion is faster than  $\propto E^1$ , interaction efficiency rapidly declines above tens of PeV. This is reasonable when a quasi-ballistic propagation is assumed instead of diffusive propagation inside the jet emission region. In the one-zone model, the efficient escape of UHECRs requires a rigidity-dependent diffusion rate, for example,  $D(E) \propto E^2$  at higher energies (N. Globus et al. 2008; D. Harari et al. 2014; M. S. Muzio et al. 2022). The resulting muon

neutrino ( $\nu_\mu + \bar{\nu}_\mu$ ) flux from  $p\gamma$  interactions is given by

$$E_\nu^2 J_\nu = (1/3)(E_\nu'^2 Q'_{\nu,p\gamma})(V'^2 \Gamma_D^2 / 4\pi d_L^2), \quad (5)$$

where the factor “1/3” accounts for neutrino oscillations, and  $Q'_{\nu,p\gamma}$  is the comoving-frame production rate of electron and muon neutrinos from charged pion decay.

The magenta curve in Figure 1 shows the resulting muon neutrino spectrum obtained using the same normalization of the proton spectrum, after accounting for neutrino oscillations. The  $\nu_\mu + \bar{\nu}_\mu$  event rate at IceCube in a given operation time  $\Delta T$  is calculated using the expression

$$\mathcal{N}_{\nu_\mu} = \Delta T \int_{\epsilon_{\nu,\min}}^{\epsilon_{\nu,\max}} d\epsilon_\nu \frac{d\Phi_\nu}{d\epsilon_\nu} \langle A_{\text{eff}} \rangle_\theta, \quad (6)$$

where  $\langle A_{\text{eff}} \rangle_\theta$  is the effective detector area averaged over the zenith angle bin concerned (IceCube Collaboration 2019a). We use the effective area for event selection as a function of neutrino energy from J. Stettner (2020). We calculate the number of muon neutrino events from this source to be  $\sim 0.1$  events in 10 yr at IceCube. It is much lower than the muon neutrino flux predicted from TXS 0506+056, assuming a 0.5 and 7 yr flux level, also shown in the figure for comparison.

We note that the maximum proton energy required to explain the observed SED is  $\simeq 4 \text{ PeV}$  in the comoving jet frame. This corresponds to the AGN rest frame proton energy of  $E_p = \Gamma E'_p = 0.1 \text{ EeV}$ . We assume protons above this energy escape the blazar jet without significant energy loss and propagate through the extragalactic medium.

### 3.2. Luminosity Requirement and LIV Coefficient

LIV in the hadronic sector is defined by the modified dispersion relation  $E_i^2 - p_i^2 = m^2 + \delta_i^{(n)} E^{2+n}$  (S. R. Coleman & S. L. Glashow 1997). The mean free path of UHECRs is significantly increased when  $\delta_{\text{had},0} > 0$ . For a choice of LIV coefficient  $\delta_{\text{had},0} = 10^{-21}$  in the leading order, a primary proton of energy  $\mathcal{O} \sim 100 \text{ EeV}$  can reach Earth from a distance corresponding to this blazar without being attenuated by photopion production; suffering energy loss only due to expansion of the Universe (see Figure 4 in Pierre Auger Collaboration 2022). This value is well within the upper limit of  $\delta_{\text{had},0} < 10^{-19}$  presented by Auger. We constrain the value of  $R_{\max}$  and hence the required LIV coefficient from the proton luminosity required to explain the blazar SED.

The detection of a single event by TA in the energy range 148–340 EeV (obtained by adding the statistical and systematic uncertainties in quadrature), assuming no interactions, provides the injected luminosity in this energy range for TA exposure  $\mathcal{E} = 1.6 \times 10^4 \text{ km}^2 \text{ sr yr}$  (Telescope Array Collaboration 2023). We use the injection spectrum per unit time in Equation (4), emitted within a solid angle  $2\pi(1 - \cos\theta_{\text{jet}})$  subtended by a typical jet opening angle of  $\theta_{\text{jet}} \approx 0.1$  radians (A. B. Pushkarev et al. 2009; J. D. Finke 2019). Using the same normalization, we can calculate the kinetic power in protons for the energy range 10 TeV up to 10 EeV, beyond which LIV effects kick in. In Figure 2, we show the luminosity required in protons as a function of the injection spectral index  $\alpha$  for different values of  $R_{\max}$ . Noting that our multiwavelength modeling requires a proton power of  $L_p = 1.3 \times 10^{45} \text{ erg s}^{-1}$  in the blazar jet (see Table 1) and a spectral index of  $\alpha = 2$ , this corresponds to a total power of  $L_p(\leq 10 \text{ EeV}) = 2 \times 10^{45} \text{ erg s}^{-1}$ . Thus, the corresponding

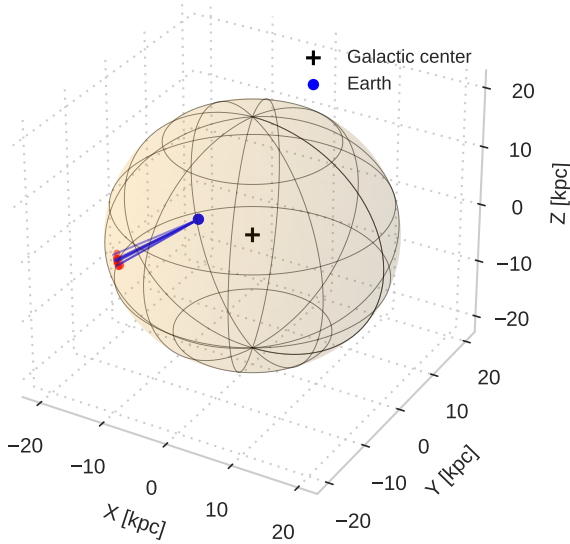


**Figure 3.** UHECR particles placed randomly on the surface of the Galactic horizon (red) for M. Unger & G. R. Farrar (2024b) magnetic field with momentum vector given by von Mises–Fisher distribution concentrated around the angular uncertainty region, centered on the best-fit direction at Earth. The black and blue dots correspond to the Galactic center and Earth. A backtracking simulation of protons from Earth to these directions shows negligible deflections in the GMF, illustrating the requirement for a high magnitude of EGMF.

value of  $\log_{10}(R_{\max}/V)$  is inferred between 19 and 19.2 from Figure 2. The value of cutoff rigidity obtained by Auger at this LIV coefficient for a generic source population, from a combined fit to the energy spectrum and composition using Sybill2.3c hadronic interaction model (F. Riehn et al. 2020) and R. C. Gilmore et al. (2012) EBL model, is  $\sim 18.6$  and increases with increasing  $\delta_{\text{had},0}$ .

### 3.3. UHECR Deflection in Cosmic Magnetic Fields

At these extreme energies, UHECRs do not lose significant energy en route to Earth (due to LIV) but may undergo deflection in cosmic magnetic fields. The angular resolution of the TA surface detector for events with  $E > 10$  EeV is  $1.4^\circ$  (J. Kim et al. 2023). To account for the directional uncertainty in the observed arrival direction of the Amaterasu event, we generate sample UHECR particles with their random momentum direction drawn from a von Mises–Fisher (vMF) distribution  $f(\theta) = \kappa \exp(\kappa \cos \theta) / 2 \sinh \kappa$ . The value of the parameter  $\kappa$  is chosen such that the particles are concentrated around the angular uncertainty region, centered on the best-fit direction at Earth. We show these directions intersecting the Galactic boundary as red points on the spherical surface in Figure 3. The Galactic boundary is considered to be an outer radius of  $\approx 20$  kpc from the Galactic center (black cross) in various magnetic field models (R. Jansson & G. R. Farrar 2012; M. Unger & G. R. Farrar 2024b).

Next, we perform a backtracking simulation of cosmic rays from Earth (blue dot in Figure 3), sampling energies given by a power-law spectrum  $dN/dE \sim E^{-2}$  between the uncertainty range 148–340 EeV. These cosmic rays are propagated with injected directions drawn from a distinct vMF sample to check the deflection at the Galactic boundary due to the Galactic magnetic field (GMF). We use the Monte Carlo simulation framework CRPROPA 3.2 for the backtracking simulation (R. Alves Batista et al. 2016, 2022). The code allows the

implementation of various magnetic field models for the propagation of UHECRs.

We adopt the UF23 model, as introduced by M. Unger & G. R. Farrar (2024b), which provides a divergence-free parameterization of the large-scale disk, toroidal halo, and poloidal (X-shaped) field components. This model is constrained by a joint fit to full-sky rotation measures and polarized synchrotron intensity maps from WMAP and Planck, using updated electron density and cosmic-ray lepton distributions. We test the 20-parameter base model as well as the local magnetic spur structure near the Sun (spur) and exponential decay (expX) models. We performed the backtracking simulation using 10 particles across 100 random realizations of the vMF. The resulting intersection points on the Galactic boundary align well with the initial vMF distribution for all models, indicating that deflections due to the GMF are negligible. Figure 3 shows that UHECRs at this energy travel along a straight line path in the Galaxy. The results were also found to be consistent with the JF2012 model (R. Jansson & G. R. Farrar 2012). Hence, the deflection from the direction of the blazar can be attributed to the extragalactic magnetic field (EGMF).

A high intensity of the EGMF is expected for the  $2.5^\circ$  deflection from the blazar. For Larmor radius  $r_L$  in the magnetic field, the expected deflection angle is  $\theta_{\text{def}} = \sqrt{2d_c \lambda_c} / 3r_L$ , assuming small-angle scattering. We calculate the required strength of EGMF and express the deflection of a UHECR with charge  $Z$  from the blazar direction in the parametric form as (C. D. Dermer et al. 2009; K. Murase 2012)

$$\theta_{\text{def}} \simeq 2.5 Z \left( \frac{d_c}{590 \text{ Mpc}} \right)^{1/2} \left( \frac{\lambda_c}{500 \text{ kpc}} \right)^{1/2} \times \left( \frac{B_{\text{EG}}}{1.54 \text{ nG}} \right) \left( \frac{E_p}{250 \text{ EeV}} \right)^{-1}, \quad (7)$$

where  $d_c = 590$  Mpc is the comoving distance to the source,  $\lambda_c$  is the turbulence coherence length, and  $B_{\text{EG}}$  is the rms strength of the EGMF. We find that  $B_{\text{EG}} \approx 1.5$  nG is required to deflect protons by  $2.5^\circ$  from the initial emission direction. The value corresponds to the magnetic field in cosmic filaments (F. Vazza et al. 2014). The Universe is not homogeneous at these distance scales, and UHECRs may encounter matter concentrated in superclusters or filaments, separated by intergalactic voids, resulting in the deflection of proton primaries.

The TA collaboration showed backtracked arrival directions assuming two GMF models, JF2012 and PT2011 (M. S. Pshirkov et al. 2011). In both cases, a plausible association with blazar PKS 1717+177 emerges only for a proton primary. For heavier nuclei, such as iron, the backtracked direction in the JF2012 model shifts toward a region of the large-scale structure populated by galaxies (see Figure 2 in Telescope Array Collaboration 2023), disfavoring the blazar hypothesis.

## 4. Discussions

Earlier studies on the broadband emission of this source imply a high Doppler factor  $\delta_D > 50$  and a low magnetic field for the SSC model. However, it is discussed that the SSC model does not provide a good fit to the LAT  $\gamma$ -ray spectrum under a one-zone leptonic model only (F. Tavecchio et al. 2010). In our work, we provide a first analysis of this source in light of leptohadronic interactions. The nuclear jet of this

source appears to be deflected and bent at about 0.5 mas distance from the radio core via gravitational lensing or the magnetosphere of a second massive black hole (S. Britzen et al. 2024, 2025). This meandering jet structure may also explain the origin of the Amaterasu event despite being positioned at an angular offset of 2°. The value of  $R_{\text{ext}} \sim 0.5$  pc presented in our analysis is large compared to the usual estimates for the BLR region  $R_{\text{BLR}} \sim L_{\text{disk},45}^{0.5}$  cm (F. Tavecchio & G. Ghisellini 2008). This may be interpreted as the emission region lying outside the BLR or at the edge, resulting in a low BLR photon density, as considered in our model.

A proton flux at the highest energy UHECR spectrum, although subdominant, cannot be ruled out and may originate from a distinct source class. Luminous AGNs or gamma-ray bursts are probable source candidates for a proton primary since heavier nuclei are more susceptible to photodisintegration in such sources (M. Unger et al. 2015; M. Kachelrieß et al. 2017; S. Das et al. 2021b). In such cases, a hard spectral index can be expected due to increased interaction in the vicinity of the source. However, we restrict ourselves to a prudent choice of  $\alpha = 2$  motivated by the first-order Fermi acceleration.

A neural network classifier at the TA collaboration excludes a photon as the primary particle at a 99.986% confidence level (Telescope Array Collaboration 2023). For both proton and iron primaries, the average propagation distance at 244 EeV is  $\approx 30$  Mpc. A comoving distance of  $\approx 590$  Mpc for the blazar source of this event can thus be reconciled with LIV effects in extragalactic propagation. The absence of other sources within the angular uncertainty region of 1.4° strengthens the case for the blazar hypothesis. For a proton primary to be associated with the blazar, a strong EGMF strength is required. The uncertainty region due to GMF becomes larger for heavier elements, making it difficult to reconcile with the blazar source. Constraints on the number density of UHECR sources emitting heavy nuclei have been studied (M. Y. Kuznetsov 2024). Moreover, in order to reproduce the observed degree of isotropy of cosmic rays at  $\sim$ EeV energies, the average magnetic field in cosmic voids must be  $\sim 0.1$  nG (S. Hackstein et al. 2016). The value we obtain is 1 order of magnitude higher, corresponding to that in filaments.

The source is located above the IceCube horizon, allowing the observation of an upgoing  $\nu_\mu$  track-like event, reducing the atmospheric background. The IceCube-Gen2 radio array (IceCube Collaboration 2019b, 2021), with 8 times more instrument volume than the current capacity, will have 5 times more sensitivity, thus increasing the chance of neutrino detection from this source. During increased X-ray and  $\gamma$ -ray activity, if the kinetic power in protons increases by 1 order of magnitude, IceCube-Gen2 will be able to detect an event within a few years of observation. The effective area of the ARCA detector of KM3NeT (KM3NeT Collaboration 2016), assuming an isotropic neutrino flux, is comparable to that of IceCube. Several other next-generation neutrino telescopes, such as TAMBO in the southern hemisphere (A. Romero-Wolf et al. 2020) and satellite-based detector POEMMA (POEMMA Collaboration 2021), will increase the sensitivity of PeV neutrinos in the northern hemisphere.

The  $\gamma$ -ray luminosity of the source obtained in our leptohadronic model in the energy range 100 MeV–100 GeV is  $L_\gamma \approx 1.1 \times 10^{45}$  erg s $^{-1}$ . The number of sources in the luminosity-redshift phase space similar to PKS 1717+177 is

very small (see Figure 1 in S. Das et al. 2021a, using the same energy range), making a significant diffuse UHECR flux excess above 10 EeV unlikely from a population of similar sources. It has been shown that resolved  $\gamma$ -ray sources are insufficient to account for the population of sources producing the highest-energy cosmic rays, and there must exist a population of UHECR sources that lack  $\gamma$ -ray emission or are unresolved by the current-generation  $\gamma$ -ray telescopes (A. Partenheimer et al. 2024). The number of detected UHECR events with  $E \gtrsim 100$  EeV is currently too small for a statistically robust correlation study with the known blazar population. No significant anisotropy has been detected at these energies (B. R. d’Orfeuille et al. 2014; Pierre Auger Collaboration 2015b), making it difficult to identify potential sources. This can be attributed to the dominance of heavier nuclei and the resulting smearing of directionality in cosmic magnetic fields (Telescope Array Collaboration 2024). Although no event similar to Amaterasu with a plausible blazar counterpart has been identified, magnetic deflections and limited statistics hinder firm conclusions.

LIV effects become significant above  $\sim 10$  EeV for our choice of  $\delta_{\text{had},0} = 10^{-21}$ . UHE protons at  $\gtrsim 0.1$  EeV up to 10 EeV, escaping the blazar jet, can interact with the CMB and EBL photons to give rise to a line-of-sight resolved cosmogenic  $\gamma$ -ray spectrum (W. Essey et al. 2011; S. Das et al. 2020). It has a universal shape for a fully developed electromagnetic cascade, peaking at TeV energies for a given injection spectrum of UHE protons. Since the EGMF is considered to be rather strong, the collimation of the UHECR beam is difficult to maintain. Hence, for an appreciable cosmogenic  $\gamma$ -ray spectrum, most of the interactions must happen near the source. If CTA or LHAASO detects a steady multi-TeV  $\gamma$ -ray flux, this may indicate cosmogenic photons, further hinting toward UHECR acceleration.

## 5. Conclusions

Our study presents a multiwavelength analysis of the blazar potentially linked to one of the highest energy UHECR events recorded using a modern state-of-the-art surface detector array. The findings weave together cosmic rays, neutrinos, and  $\gamma$ -rays into a unified multimessenger narrative. Our analysis also uncovers a novel probe of beyond Standard Model physics through the possible imprints of Lorentz invariance violation. We show that UHE protons from this source can be deflected by a few degrees, arriving at Earth for a sufficiently strong EGMF. The interaction of the proton spectrum within the jet may lead to a detectable signature in the soft X-ray and sub-TeV  $\gamma$ -ray spectrum. The neutrino flux obtained in the steady state has a low event rate, making it difficult to detect by the exposure of currently operating detectors. However, our analysis suggests that next-generation neutrino telescopes can constrain UHECR acceleration from this source within a few years of observation, particularly if an increased activity is observed in X-ray or  $\gamma$ -ray wave band. This source provides strong motivation for a dedicated multiwavelength and multimessenger campaign.


## Acknowledgments

Numerical computations in this work were carried out at the Raman Research Institute computing facility.



*Software:* GAMERA (J. Hahn 2016; J. Hahn et al. 2022), CRPropa 3.2 (R. Alves Batista et al. 2016, 2022).

## ORCID iDs

Saikat Das  <https://orcid.org/0000-0001-5796-225X>  
 Srijita Hazra  <https://orcid.org/0009-0007-0381-8069>  
 Nayantara Gupta  <https://orcid.org/0000-0002-1188-7503>

## References

- Abbasi, R. U., Abu-Zayyad, T., Al-Seady, M., et al. 2010, *PhRvL*, **104**, 161101
- Aloisio, R., Berezhinsky, V., & Gazizov, A. 2012, *APh*, **129**, 39
- Alves Batista, R., Becker Tjus, J., Dörner, J., et al. 2022, *JCAP*, **09**, 035
- Alves Batista, R., Dundovic, A., Erdmann, M., et al. 2016, *JCAP*, **05**, 038
- Anchoroqui, L. A. 2019, *PhR*, **801**, 1
- Ansoldi, S., Antonelli, L. A., Arcaro, C., et al. 2018, *ApJL*, **863**, L10
- Atoyan, A., & Dermer, C. D. 2001, *PhRvL*, **87**, 221102
- Ballet, J., Bruel, P., Burnett, T. H., Lott, B., & The Fermi-LAT collaboration 2023, *arXiv:2307.12546*
- Barnacka, A., Moderski, R., Behera, B., Brun, P., & Wagner, S. 2014, *A&A*, **567**, A113
- Becker, R. H., White, R. L., & Helfand, D. J. 1994, in ASP Conf. Ser. 61, *Astronomical Data Analysis Software and Systems III*, ed. D. R. Crabtree, R. J. Hanisch, & J. Barnes (San Francisco, CA: ASP), 165
- Berezinskii, V. S., & Ginzburg, V. L. 1981, *MNRAS*, **194**, 3
- Bianchi, L., Herald, J., Efremova, B., et al. 2011, *Ap&SS*, **335**, 161
- Bird, D. J., Corbato, S. C., Dai, H. Y., et al. 1995, *ApJ*, **441**, 144
- Boettcher, M., Reimer, A., Sweeney, K., & Prakash, A. 2013, *ApJ*, **768**, 54
- Boettcher, M., & Schlickeiser, R. 1997, *A&A*, **325**, 866
- Bourriche, N., & Capel, F. 2024, *arXiv:2406.16483*
- Britzen, S., Kovačević, A. B., Zajaček, M., et al. 2024, *MNRAS*, **535**, 2742
- Britzen, S., Böttcher, M., Kun, E., et al. 2025, *A&A*, **695**, A103
- Chodorowski, M. J., Zdziarski, A. A., & Sikora, M. 1992, *ApJ*, **400**, 181
- Coleman, S. R., & Glashow, S. L. 1997, *PhLB*, **405**, 249
- Das, S., Gupta, N., & Razzaque, S. 2020, *ApJ*, **889**, 149
- Das, S., Gupta, N., & Razzaque, S. 2021a, *ApJ*, **910**, 100
- Das, S., Gupta, N., & Razzaque, S. 2022a, *A&A*, **668**, A146
- Das, S., Razzaque, S., & Gupta, N. 2021b, *EPJC*, **81**, 59
- Das, S., Razzaque, S., & Gupta, N. 2022b, *A&A*, **658**, L6
- Dermer, C. D., Razzaque, S., Finke, J. D., & Atoyan, A. 2009, *NJPh*, **11**, 065016
- d'Orfeuil, B. R., Allard, D., Lachaud, C., et al. 2014, *A&A*, **567**, A81
- Ehlert, D., van Vliet, A., Oikonomou, F., & Winter, W. 2024, *JCAP*, **02**, 022
- Eichler, D. 1979, *ApJ*, **232**, 106
- Essey, W., Kalashev, O., Kusenkov, A., & Beacom, J. F. 2011, *ApJ*, **731**, 51
- Fargion, D., De Sanctis Lucentini, P. G., & Khlopov, M. Y. 2024, *Univ*, **10**, 323
- Farrar, G. R. 2025, *PhRvL*, **134**, 081003
- Fermi-LAT Collaboration 2020, *ApJS*, **247**, 33
- Finke, J. D. 2019, *ApJ*, **870**, 28
- Gilmore, R. C., Somerville, R. S., Primack, J. R., & Dominguez, A. 2012, *MNRAS*, **422**, 3189
- Giommi, P., Polenta, G., Lähteenmäki, A., et al. 2012, *A&A*, **541**, A160
- Globus, N., Allard, D., & Parizot, E. 2008, *A&A*, **479**, 97
- Gould, R. J., & Schröder, G. P. 1967, *PhRv*, **155**, 1404
- Greisen, K. 1966, *PhRvL*, **16**, 748
- Gueta, O. 2021, *ICRC (Berlin)*, **395**, 885
- Hackstein, S., Vazza, F., Brüggén, M., Sigl, G., & Dundovic, A. 2016, *MNRAS*, **462**, 3660
- Hahn, J. 2016, *PoS, ICRC2015*, 917
- Hahn, J., Romoli, C., & Breuhaus, M. 2022, GAMERA: Source modeling in gamma astronomy. Astrophysics Source Code Library, *ascl:2203.007*
- Harari, D., Möllerach, S., & Roulet, E. 2014, *PhRvD*, **89**, 123001
- Healey, S. E., Romani, R. W., Taylor, G. B., et al. 2007, *ApJS*, **171**, 61
- IceCube Collaboration 2018, *Sci*, **361**, 147
- IceCube Collaboration 2019a, *EPJC*, **79**, 234
- IceCube Collaboration 2019b, *BAAS*, **51**, 288
- IceCube Collaboration 2021, *JPhG*, **48**, 060501
- IceCube Collaboration, Fermi-LAT Collaboration, MAGIC Collaboration, et al. 2018, *Sci*, **361**, eaat1378
- Jansson, R., & Farrar, G. R. 2012, *ApJ*, **757**, 14
- Jiang, X., Liao, N.-H., Rui, X., Fan, Y.-Z., & Wei, D.-M. 2025, *ApJ*, **986**, 110
- Kachelrieß, M., Kalashev, O., Ostapchenko, S., & Semikoz, D. V. 2017, *PhRvD*, **96**, 083006
- Kawamuro, T., Ueda, Y., Shidatsu, M., et al. 2018, *ApJS*, **238**, 32
- Keivani, A., Murase, K., Petropoulou, M., et al. 2018, *ApJ*, **864**, 84
- Kelner, S. R., & Aharonian, F. A. 2008, *PhRvD*, **78**, 034013
- Kim, J., Ivanov, D., Jui, C., & Thomson, G. 2023, *EPJWC*, **283**, 02005
- KM3NeT Collaboration 2016, *JPhG*, **43**, 084001
- Kotera, K., & Olinto, A. V. 2011, *ARA&A*, **49**, 119
- Kuznetsov, M. Y. 2024, *JCAP*, **04**, 042
- Lang, R. G. 2024, *JCAP*, **11**, 023
- Mannheim, K., Stanev, T., & Biermann, P. L. 1992, *A&A*, **260**, L1
- Mücke, A., Engel, R., Rachen, J. P., Protheroe, R. J., & Stanev, T. 2000, *CoPhC*, **124**, 290
- Murase, K. 2012, *ApJL*, **745**, L16
- Murase, K., Inoue, Y., & Dermer, C. D. 2014, *PhRvD*, **90**, 023007
- Murase, K., Narita, Y., & Yin, W. 2025, *arXiv:2504.15272*
- Murase, K., & Stecker, F. W. 2023, The Encyclopedia of Cosmology. Set 2: Frontiers in Cosmology. Volume 2: Neutrino Physics and Astrophysics (Singapore: World Scientific), 483
- Muzio, M. S., Farrar, G. R., & Unger, M. 2022, *PhRvD*, **105**, 023022
- Muzio, M. S., Unger, M., & Farrar, G. R. 2019, *PhRvD*, **100**, 103008
- Nieppola, E., Tornikoski, M., Lähteenmäki, A., et al. 2007, *AJ*, **133**, 1947
- Pierre Auger Collaboration 2015a, *NIMPA*, **798**, 172
- Pierre Auger Collaboration 2015b, *ApJ*, **804**, 15
- Pierre Auger Collaboration 2017, *JCAP*, **04**, 038
- Pierre Auger Collaboration 2022, *JCAP*, **01**, 023
- POEMMA Collaboration 2021, *JCAP*, **06**, 007
- Padovani, P., Oikonomou, F., Petropoulou, M., Giommi, P., & Resconi, E. 2019, *MNRAS*, **484**, L104
- Partenheimer, A., Fang, K., Alves Batista, R., & Menezes de Almeida, R. 2024, *ApJL*, **967**, L15
- Planck Collaboration, Ade, P. A. R., Aghanim, N., et al. 2014, *A&A*, **571**, A28
- Prince, R., Das, S., Gupta, N., Majumdar, P., & Czerny, B. 2024, *MNRAS*, **527**, 8746
- Pshirkov, M. S., Tinyakov, P. G., Kronberg, P. P., & Newton-McGee, K. J. 2011, *ApJ*, **738**, 192
- Pushkarev, A. B., Kovalev, Y. Y., Lister, M. L., & Savolainen, T. 2009, *A&A*, **507**, L33
- Riehn, F., Engel, R., Fedynitch, A., Gaisser, T. K., & Stanev, T. 2020, *PhRvD*, **102**, 063002
- Romero-Wolf, A., Alvarez-Muñiz, J., Carvalho, W. R., Jr., et al. 2020, *arXiv:2002.06475*
- Sarmah, P., Das, N., Borah, D., Chakraborty, S., & Mehta, P. 2025, *PhRvD*, **111**, 083048
- Sigl, G., Miniati, F., & Ensslin, T. A. 2004, *PhRvD*, **70**, 043007
- Sikora, M., Kirk, J. G., Begelman, M. C., & Schneider, P. 1987, *ApJL*, **320**, L81
- Stecker, F. W. 1968, *PhRvL*, **21**, 1016
- Stecker, F. W., Done, C., Salamon, M. H., & Sommers, P. 1991, *PhRvL*, **66**, 2697
- Stettner, J. 2020, *ICRC (Madison, WI)*, 358, 1017
- Stratta, G., Capalbi, M., Giommi, P., et al. 2011, *arXiv:1103.0749*
- Szabo, A. P., & Protheroe, R. J. 1994, *Aph*, **2**, 375
- Telescope Array Collaboration 2016, *Aph*, **80**, 131
- Telescope Array Collaboration 2023, *Sci*, **382**, abo5095
- Telescope Array Collaboration 2024, *PhRvL*, **133**, 041001
- Tavecchio, F., & Ghisellini, G. 2008, *MNRAS*, **386**, 945
- Tavecchio, F., Ghisellini, G., Ghirlanda, G., Foschini, L., & Maraschi, L. 2010, *MNRAS*, **401**, 1570
- Tully, R. B., Shaya, E. J., Karachentsev, I. D., et al. 2008, *ApJ*, **676**, 184
- Unger, M., & Farrar, G. R. 2024a, *ApJL*, **962**, L5
- Unger, M., & Farrar, G. R. 2024b, *ApJ*, **970**, 95
- Unger, M., Farrar, G. R., & Anchoroqui, L. A. 2015, *PhRvD*, **92**, 123001
- Vazza, F., Brüggén, M., Gheller, C., & Wang, P. 2014, *MNRAS*, **445**, 3706
- Vernetto, S. 2016, *JPhCS*, **718**, 052043
- Wright, A., & Otrupcek, R. 1992, *BICDS*, **41**, 47
- Wright, E. L., Eisenhardt, P. R. M., Mainzer, A. K., et al. 2010, *AJ*, **140**, 1868
- Zatsepin, G. T., & Kuz'min, V. A. 1966, *JETPL*, **4**, 78
- Zhang, B. T., Murase, K., Ekanger, N., Bhattacharya, M., & Horiuchi, S. 2024, *arXiv:2405.17409*